npj | biofilms and microbiomes

Article

Published in partnership with Nanyang Technological University

https://doi.org/10.1038/s41522-025-00892-7

High-resolution visualization of biofilm matrix development in space and time using fluorescent stains for cellulose

Zaira Heredia-Ponce, Aurélien Bailly ✉ & Leo Eberl ✉

The establishment of microbial biofilms, communities embedded in self-produced extracellular matrices, poses growing challenges for health and antimicrobial management. Understanding biofilm formation is crucial for developing control and eradication strategies. In response to environmental cues, planktonic bacteria adopt a sessile lifestyle, coordinating growth with matrix production. We monitored cellulose biofilm formation by *Pseudomonas sp*. IsoF in real time using single-step fluorescent stains. Live-tracking of polysaccharide synthesis revealed dynamic matrix arrangements shaping final biofilm structure. Cellulose determined substratum adherence, cell contacts, and colony patterning in IsoF. Biofilms formed in flow-cells and at air-liquid interfaces were remarkably similar in composition, progression, and architecture. Artificial elevation of intracellular c-di-GMP levels produced cellulose-dependent biofilms distinct from the wild type and induced a secondary exopolysaccharide. Our fluorescent probes provide real-time visualization of matrix development, enabling detailed analysis of biofilm architecture and regulation in standard laboratory conditions.

Bacterial biofilms are complex and structured cell communities that colonize surfaces or interfaces and are encased in self-produced extracellular matrices (ECM)[1]. The biofilm mode of growth has been suggested to be the dominant lifestyle of bacteria and has been found on all kinds of natural and artificial surfaces[2]. These structures play roles that range from beneficial to harmful, depending on the microorganism involved and the contextual conditions in which they form[3–5]. Very frequently, biofilms have a significant negative impact in the medical and food industries, leading to infections and acting as reservoirs for pathogenic bacteria, respectively[6,7]. In medical settings, biofilms can develop chronic, nosocomial, and medical device-related infections, as well as oral diseases, and it has been well demonstrated that bacterial resistance to antibiotics and host immune responses are enhanced in biofilms[8,9].

The ECM is of paramount importance in biofilms, as it provides the structural framework that enables the formation and stability of these microbial communities, including its emerging properties, such as resilience to adverse environmental conditions and increased resistance to antibiotics[10,11]. For instance, the ECM is crucial for the formation of the mushroom-shaped structures in the opportunistic human pathogen *Pseudomonas aeruginosa*. These three-dimensional protrusions emerge from the biofilm's surface and are integral to its overall architecture[12,13]. Although research over the past two decades has confirmed that biofilms consist of densely packed cells enmeshed within their ECM, as exemplified by the *P. aeruginosa* model, there remains a significant gap in our understanding of the precise mechanisms underlying ECM development. Although time-resolved, high-resolution imaging has become essential for studying bacterial population behaviors in biofilm formation, routine approaches commonly rely on fluorescently labeled cells to reveal dynamic changes over time. However, it is assumed that the ECM, as an integral component of biofilms, also undergoes significant spatiotemporal changes during development. Despite its importance, tools for visualizing matrix dynamics with comparable resolution remain limited, hindering a more comprehensive understanding of the biofilm maturation. Addressing these gaps requires accessible and cost-effective imaging techniques that can distinguish between different matrix components, coupled with downstream analytical methods. The lack of mechanistic insight into matrix production hinders a full understanding of the biofilm formation process and could limit the development of more effective strategies for their control or prevention. This study aimed to fill these gaps by using the *Pseudomonas* sp. IsoF (IsoF) strain as a model, an environmental isolate from tomato roots[14] extensively studied in our laboratory. IsoF exhibits remarkable rhizocompetence and biocontrol activity against a broad spectrum of bacteria via a type IVB secretion system-mediated contact-dependent killing mechanism[15]. As this obligate aerobic strain forms biofilms in various laboratory conditions, it served as a valuable model for studying quorum sensing-regulated phenotypes[14,16,17] and is a safe alternative model to opportunistic human pathogens. The IsoF's fully sequenced genome, amenable to genetic editing and free of prophages[18], further enhances its suitability for studying community development under controlled

Department of Plant and Microbial Biology, University of Zurich, Zurich, Switzerland. ✉e-mail: aurelien.bailly@botinst.uzh.ch; leberl@botinst.uzh.ch

conditions. Although our research group has accumulated a considerable amount of data regarding the multifaceted communal behaviors exhibited by IsoF and has access to its genome, prior to this study we were unaware of the genetic information encoding potential matrix components in this strain.

We here leveraged the identification of one-step fluorescent probes to investigate the role of different polysaccharides of IsoF in biofilm formation across three prominent in vitro models: flow-cell chambers, macrocolonies and pellicles. Notably, we conducted high-resolution temporal and spatial analysis of polysaccharide production during biofilm formation in flow-cell chambers. With remarkable access to detailed temporal data on ECM production, we further investigated the architectural shifts arising from polysaccharide synthesis modulation through alterations in c-di-GMP signaling. Overall, our study provides detailed insights into ECM production, paving the way for similar investigations in other bacterial species and/or strains and their environmental adaptation.

Results

Pseudomonas sp. IsoF biofilm developmental sequence involves two consecutive cell populations

In our flow-cell system, IsoF develops a mature biofilm within 72 h of growth. Typically, the bacterial population displays an uneven topography along the channel, with high cell density and large cell aggregates close to the inlet and lower cell density and smaller cell aggregates from about the middle of the channel towards the outlet (Fig. 1A). This distribution pattern presumably reflects nutrient and oxygen gradients along the channel[19]. Between the larger cell aggregates we observed a uniform and shallow mat of cells (Fig. 1A). By monitoring biofilm development of IsoF at high temporal resolution, we were able to distinguish two discrete subpopulations: (1) founder cells (FCs), which are cells that irreversibly attach to the glass surface during inoculation; when the nutrient flow is started, FCs rapidly divide and form cell aggregates; (2) late settlers (LSs), which are cells that colonize the void spaces between the aggregates (Fig. 1B). LSs appear after FC aggregates have been formed (Fig. 1B–D). After irreversible attachment to the surface, LSs divide and grow at similar rates as FC colonies (Fig. 1B–D). We observed that LSs are FC daughter cells that leave the FC microcolonies (Fig. 1C, Video S1). The final dimensions of the FC aggregates and the positioning and development of the LS aggregates depend on space constraints. We obtained the largest microcolonies (maximum 60 µm diameter) when inoculum concentrations were lower, and a uniform mat of cells when FCs initially covered the whole glass surface (Fig. S1). We also observed that adjacent FC aggregates can connect and fuse if the contact between the growing microcolonies occurs early during biofilm development. Greater initial distances between FC cells discourage fusion events, so that the collision of mature FC aggregates results in distinct microcolonies.

Identification of fluorescent probes suitable for high-quality matrix visualization

Using IsoF pellicles (i.e., biofilms forming at the air-liquid interface of static liquid cultures) as starting material, we next screened an in-house library of fluorophores presumptively targeting polysaccharides and selected the candidate molecules Fluorescent Brightener 134 (compound (**1**)) and Tubantin Scarlet 4 G (compound (**2**)) based on their ability to stain fibers present in the biofilm matrix with suitable quantum yield and photostability. Staining 3-days old flow-cell biofilms of IsoF with these fluorescent probes allowed us to observe that the cell aggregates formed by the FCs are embedded into a fibrous biopolymer and interconnected into a network of cell-associated and cell-free fibers (Fig. 2A–C, Fig. S2A). This network covers the entire glass surface and is composed of regularly spaced (mean distance 12.1 ± 4.5 µm; Fig. S2B) and interconnected LS cell aggregates (Fig. S2C, D). High-resolution microscopy revealed that the bacterial population inside the larger aggregates is tightly enmeshed within the polymer lattice (mean pore size 1.6 ± 1.3 µm; Fig. 2D) and not motile; the matrix network embedding large aggregates resembles a 3D-filled fishnet tote bag attached to the glass surface by fibers. However, IsoF cells keep the ability to leave the microcolonies when stressed, as observed during prolonged CLSM acquisitions with 405 nm laser excitation (Video S2). We did not observe voids or cavities in these structures, as described earlier for old *P. aeruginosa* PAO1 (PAO1) biofilms[20], which might correlate with the fact that IsoF does not contain prophages in its genome and consequently shows very limited lysis and eDNA release[18–21].

Our observations are reminiscent of polysaccharide networks as demonstrated previously by the use of fluorescently-labeled lectins and CLSM[20,22] or electron microscopy[23]. A bioinformatic analysis identified three gene clusters in IsoF that potentially encode polysaccharides: (1) an alginate operon (*PisoF_02546-PisoF_02557*), (2) a *pea* operon (*PisoF_04500-PisoF_04518*) and 3) a *bcs* operon (*PisoF_03916-PisoF_03924*) sharing strong homology with the *P. putida* KT2440 (KT2440) genomic regions *PP_1277-PP_1288*, *PP_3132-PP_3142* and *PP_2629-PP_2638*, respectively (Fig. 1E)[24]. Notably, homologs of the *psl* (*PA2231-PA2244*) and *pel* (*PA3058-PA3064*) operons of PAO1 or the *peb* operon of KT2440 (*PP1795-PP1788*) were not found in the IsoF genome. This analysis also revealed that the KT2440 *bcs* operon contains a nonsense mutation resulting from a G insertion, which causes a frameshift in *bcsE* (position 418 in *PP_2629*). This subunit of the cellulose synthase complex is essential for optimal cellulose production[25], thus questioning the capacity of KT2440 to produce this polymer.

The fluorescent probes are specific to cellulose, the primary matrix exopolysaccharide in *Pseudomonas sp.* IsoF biofilms

To determine the nature of the stained polymer in IsoF, we generated single, double, and triple mutants in the three putative polysaccharide gene clusters. Three-days old biofilms of the cellulose deficient mutant (Δ*bcsA*) could not be stained with the fluorescent probes and showed a severe impairment in biofilm architecture compared to the wildtype (Fig. 3). In flow-cells, Δ*bcsA* formed a dissociated monolayer of cells without cell aggregates (Fig. 3A). Overnight treatment of the wildtype biofilm with cellulase released cells from the digested matrix, suggesting that the polymer is likely a polysaccharide with putative (1 → 4)-β-D-glucosidic linkages (Video S3). Further, the stained EPS was still formed by the IsoF alginate (Δ*alg8*) and Pea (Δ*pea*) mutants and remained sensitive to cellulase treatments (Fig. 3A). Our data provide thus strong evidence that cellulose is the principal component of IsoF's ECM in the tested flow-cell conditions. To ascertain that our stains do label celluloses, we exploited the well-characterized *Pseudomonas syringae* pv. syringae UMAF0158 strain (PssUMAF0158) and its derived biofilm polysaccharide mutants[26]. This bacterium possesses an alginate operon, a *wss* cellulose operon and a *psl*-like operon[26]. Flow-cell biofilms of PssUMAF0158 mutants unable to produce cellulose (Δ*wssE*) did not display specific fluorescence in the presence of compound (**1**) (Fig. 3B, C) or compound (**2**) (Fig. 3D, E), despite the obvious presence of surface-attached cell aggregates. Conversely, the PssUMAF0158 wild-type strain and its alginate (Δ*alg8*) and Psl (Δ*pslE*) deletion mutants exhibit a stained matrix that resembles the architecture observed in IsoF biofilms (Fig. 3B, D). When growing flow-cell biofilms of various *Pseudomonas* sp. and Betaproteobacteria in the presence of compound (**1**), we observed fluorescent matrix signals in strains predicted by bioinformatics to enable the production of cellulosic materials (Fig. S3A). Finally, mixed-species biofilms of IsoF and *P. chlororaphis* PCL1606, a strain producing Psl as principal exopolysaccharide[27], only displayed cellulosic fibers associated with IsoF aggregates in the presence of the fluorescent probes (Fig. S3B). Taken together, these data unambiguously demonstrate the suitability of the stains to specifically label cellulose.

The cellulose-specific fluorescent probes allow live-imaging of matrix biogenesis in *Pseudomonas sp.* IsoF

With these tools in hands, we initially ensured that our two fluorescent probes are not toxic for IsoF cells under our experimental conditions (Fig. S4). The lack of toxicity allowed us to visualize cellulose during biofilm development in real time. CSLM unveiled cellulose production on the glass surface promptly after the irreversible attachment of FCs (Fig. S5). When these surface-attached cells divided, they deposited cellulosic material onto the substratum, anchoring the nascent colony (Fig. S5). The fluorescent signal indicative of cellulose production lags until about 6 h of FC growth

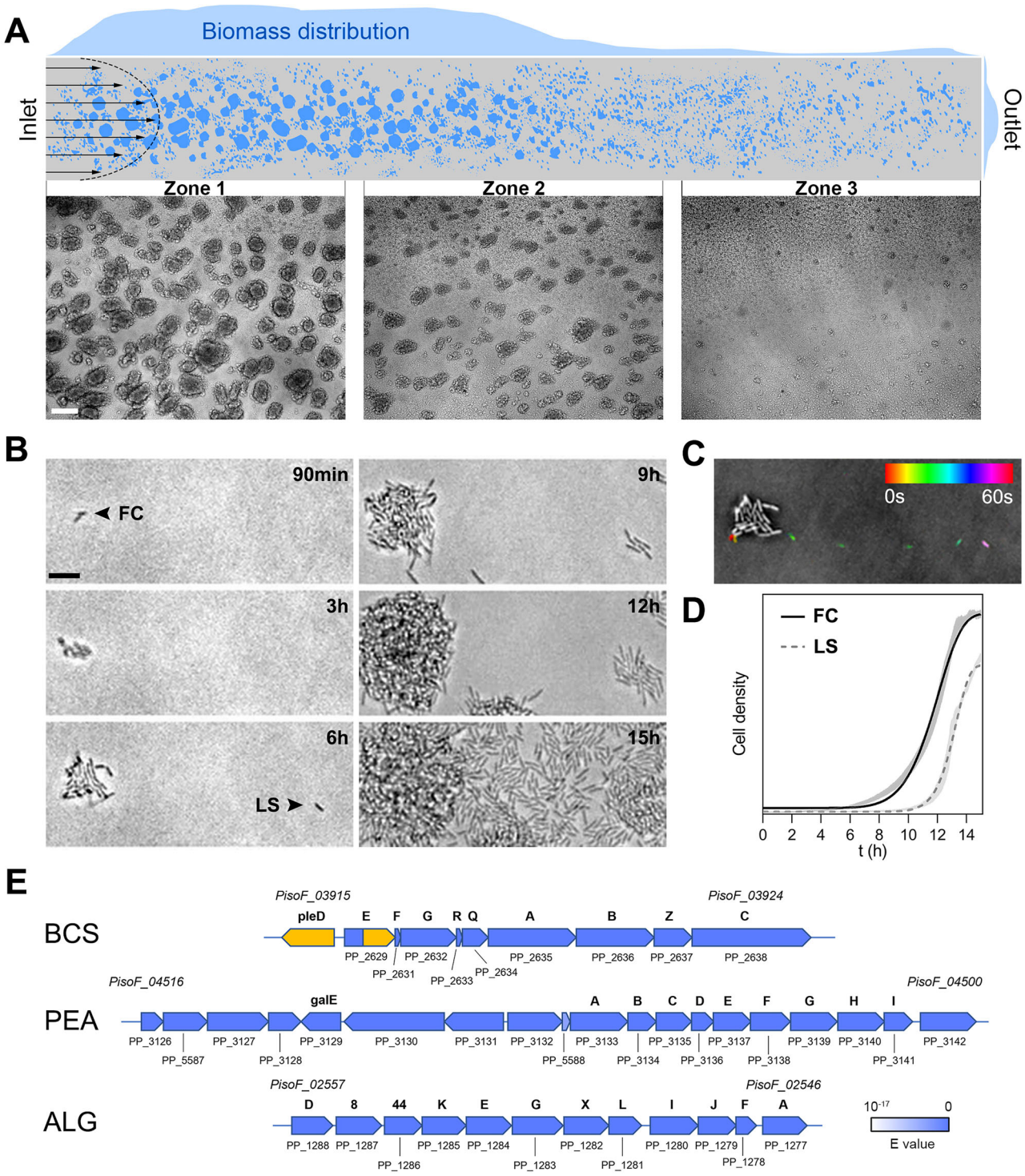

Fig. 1 | Biofilm structural development of *Pseudomonas* sp. IsoF cultivated in a flow-cell. A Schematic diagram depicting a typical distribution of IsoF microcolonies along the flow-cell channel. The micrographs shown below are representative of the indicated areas. Bar = 100 µm (**B**) Development of a microcolony following attachment of a single founder cell (FC) in time. Some cells leave the FC microcolonies, attach to an uncolonized region of the substratum and form a second generation microcolony (late settler, LS). Bar = 10 µm (**C**) Temporal color-coded projection of B. depicting the trajectory of a single LS. **D** Mean growth curves of FC and LS aggregates as estimated from micrographs; Weibull growth least square fit. Gray areas represent the standard error of the fitted data ($n = 8$). **E** Three gene clusters encoding for the production of exopolysaccharides, namely cellulose (BCS), Pea (PEA) and alginate (ALG), were identified in IsoF. Blue shades indicate E-values for orthologs in the reference *P. putida* KT2440 genome, underlining a high degree of conservation between both strains; yellow indicates missing coding sequences in KT2440.

and appears synchronously among cell aggregates reaching 9.94 µm diameter (± 7.4 µm, approx. 15–20 cells) (Video S4). During further expansion of cell aggregates, the cellulosic material at the cell-substratum interface reorganized into fibers (Fig. S6, Video S5), eventually forming a lattice. These connections span the entire glass surface, creating a cohesive network that links large and small cell aggregates, right down to individual cells. The matrix formed by aggregates develops isotropically until about 12 h of growth, followed by an apparent self-organization into tensioned fibers,

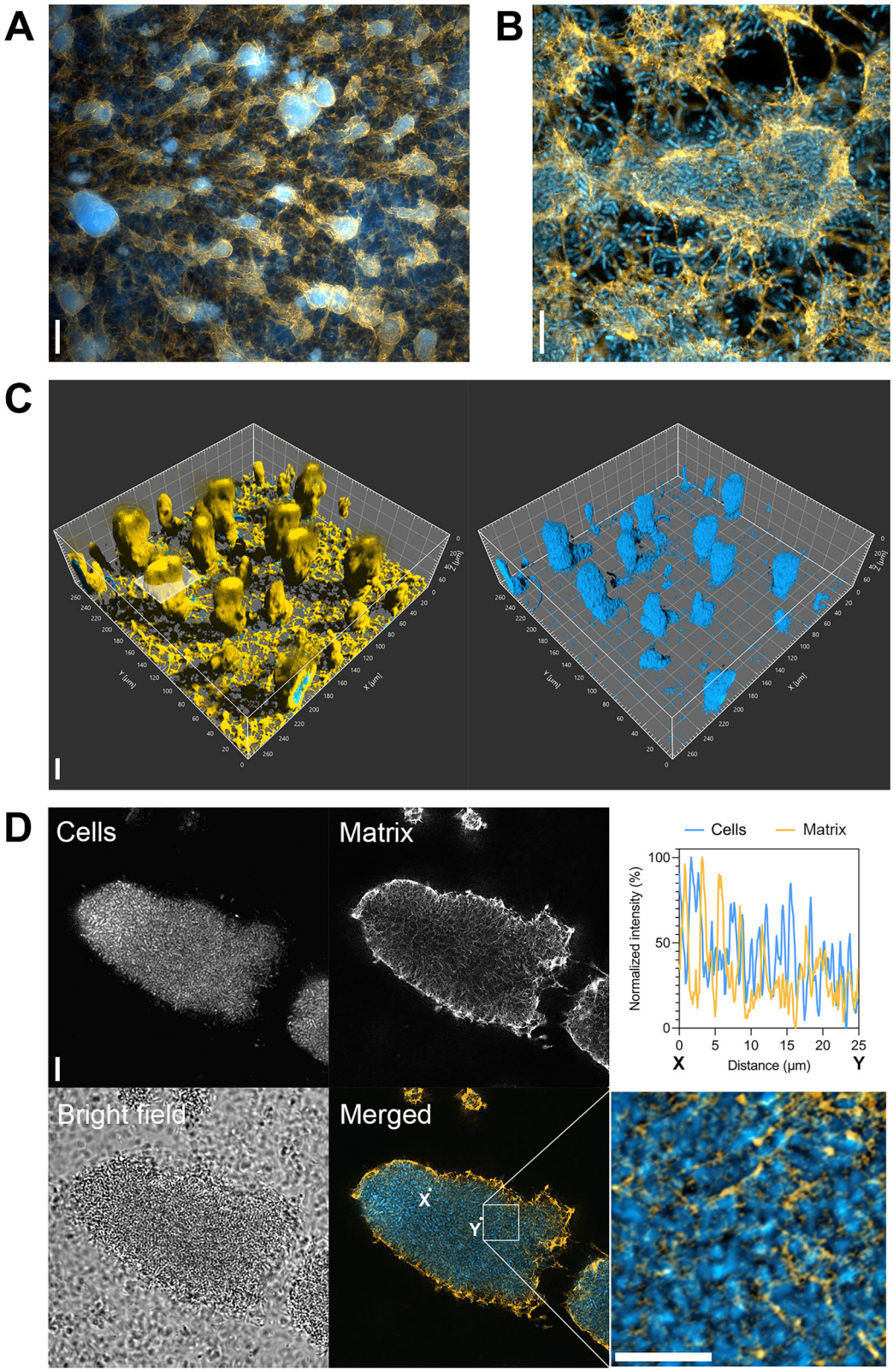

Fig. 2 | The fluorescent probes reveal the fibrous network supporting IsoF matrix architecture. IsoF cells are shown in blue, the biofilm matrix in yellow. **A** Low magnification epifluorescence micrograph showing a representative 3-days old biofilm grown in Zone 1 (Fig. 1A). Note the extended network of fibers connecting the microcolonies. Bar = 50 µm. **B** A CLSM close-up view showing a microcolony embedded in matrix material. The focal plane is the liquid-glass interface. Contrast has been adjusted for clarity. Bar = 10 µm. **C** Shadow projections showing FC aggregates and the interconnected matrix covering the substratum. The section plane is observed in D. Bar = 20 µm. **D** A CLSM optical section of a FC aggregate showing inner bacteria enmeshed into a tight matrix of fibers. The magnified region has been processed for clarity. The cells and matrix fluorescent signals do not overlap, and no gaps are observed between IsoF cells and the matrix, as quantified in the adjacent graph. Bars = 10 µm.

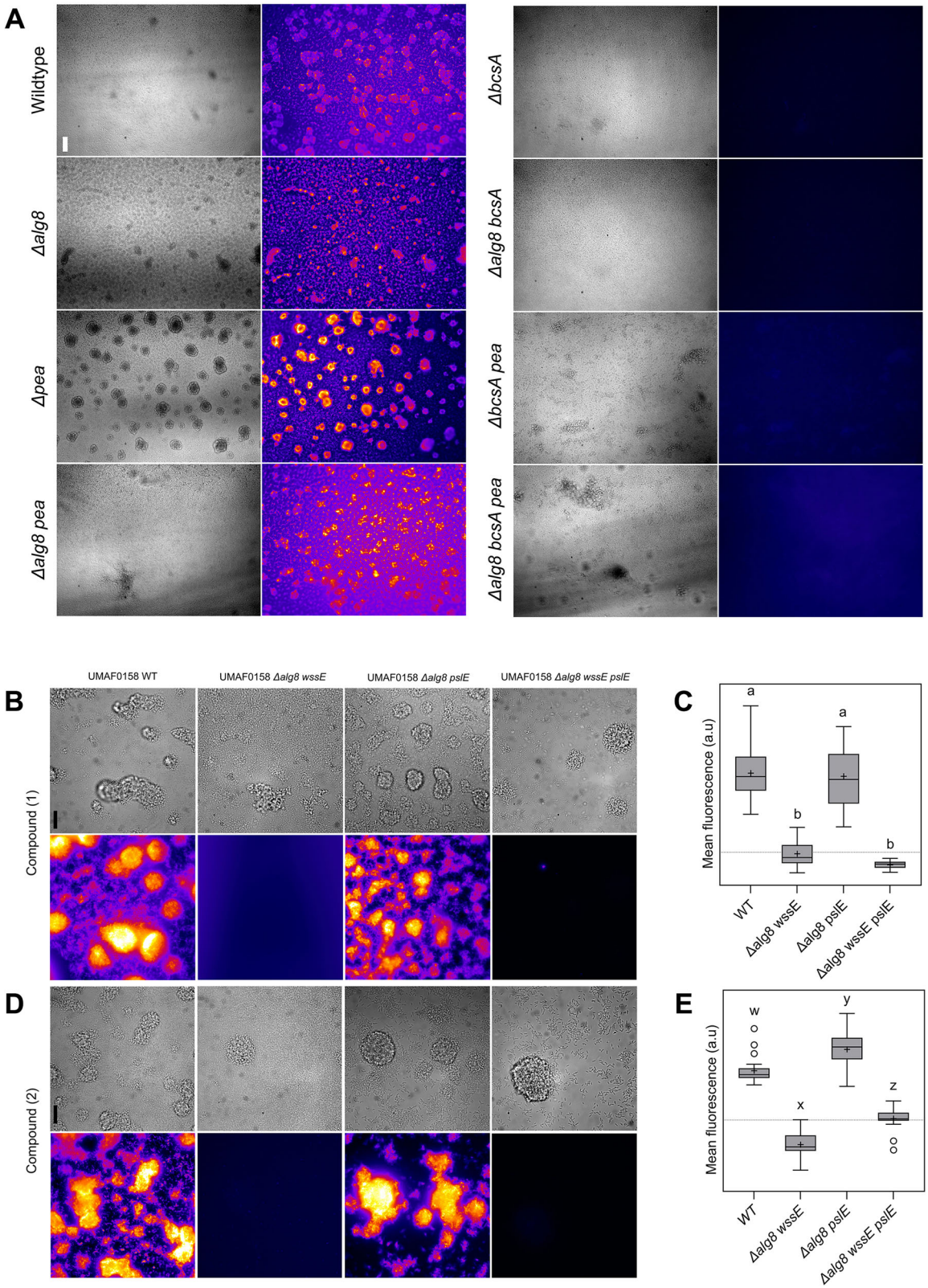

Fig. 3 | Both fluorescent probes specifically label cellulose in IsoF and PssUMAF1058 biofilms grown in flow-cell chambers. A Representative epifluorescence micrographs of 3-days old wildtype and mutant IsoF biofilms. Bright Field, Grayscale, and corresponding cellulose fluorescence in the presence of compound (1), Fire LUT. Bar = 50 µm. **B**, **C** Representative epifluorescence micrographs and total fluorescence quantifications ($n = 40$) of 3-days old biofilms of the PssUMAF0158 wildtype and its derived polysaccharide mutants in the presence of compound (**1**). **D**, **E** Representative epifluorescence micrographs and total fluorescence quantifications ($n = 20$) of 3-days old biofilms of the PssUMAF0158 wildtype and its derived polysaccharide mutants in the presence of compound (**2**). Bar = 20 µm. Different letters indicate statistically significant differences ($p \leq 0.05$) according to one-way ANOVA followed by Tukey post-hoc test.

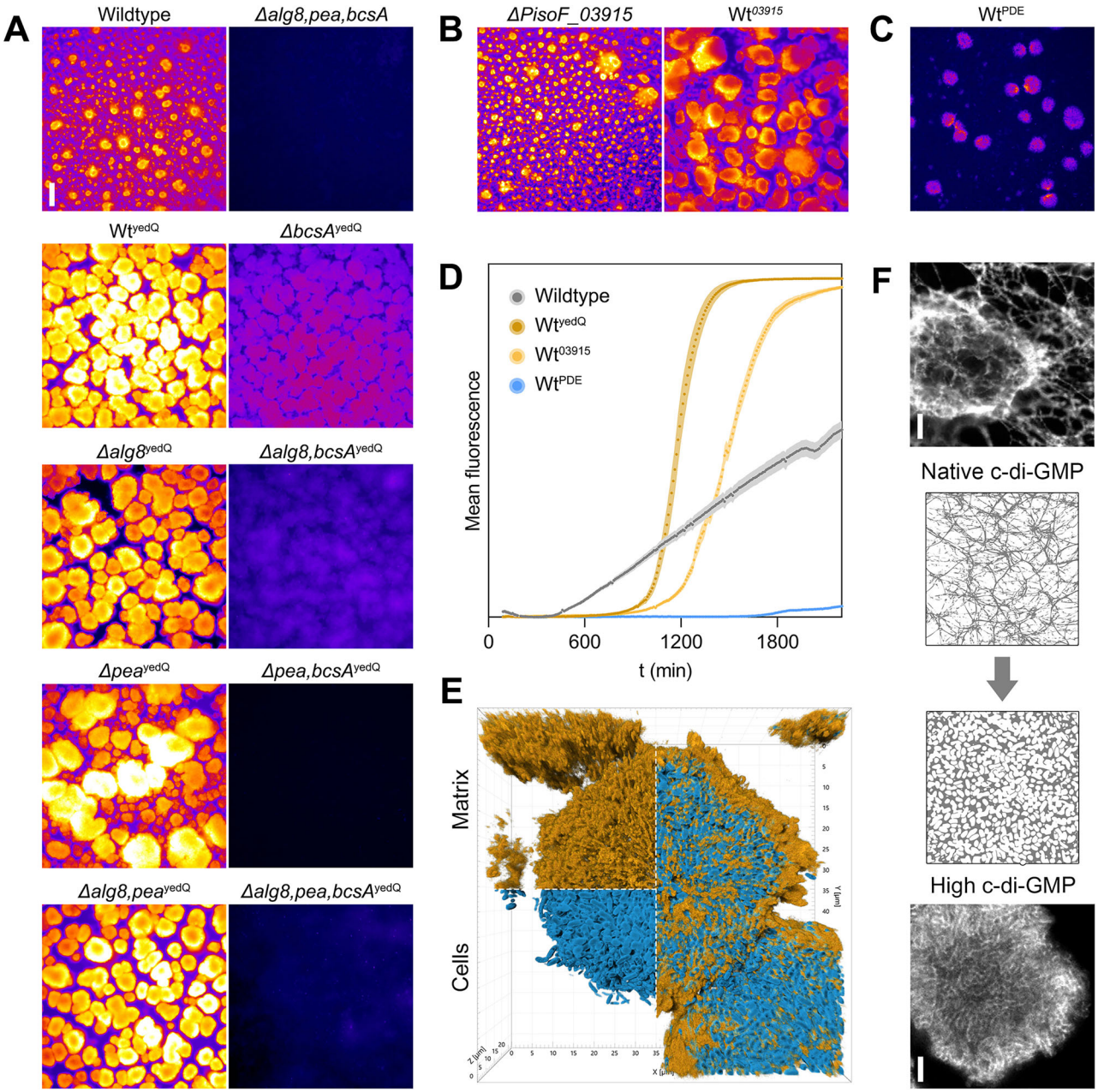

Fig. 4 | The fluorescent probes allow direct evaluation of c-di-GMP-controlled shifts in IsoF matrix production and architecture. A Topographies of the wildtype and given mutant strains under native or high c-di-GMP conditions. Note that Pea overproduction appears to compensate for the lack of cellulose (Δ*alg8,bcsA*^{yedQ}), leading to a dense biofilm topography. Compound (**1**) fluorescence, Fire LUT. Bar = 50 µm. Representative 3-days old biofilms are shown. **B** The deletion of *PisoF_03915* does not affect matrix architecture; however, its overexpression (Wt^{03915}) leads to a high c-di-GMP topography similar to the one of WT^{yedQ}. **C** Typical Wt^{PDE} biofilm. **D** Matrix cellulose production measured by fluorescence over time in native, low and high c-di-GMP conditions (n = 10, mean and s.e.m. (shades) are represented). **E** Shadow projection of a mature Wt^{yedQ} colony. Bacteria are shown in blue, the biofilm matrix in yellow. **F** Matrix architectures of native (top) and high c-di-GMP (bottom) flow-cell colonies; cellulose fluorescence. Bar = 5 µm. The diagrams depict the shift from an open to a dense network induced by elevated c-di-GMP levels; the matrix is represented in gray.

creating a 3D homotypic lattice structure. Analysis of 3D time-lapses shows that during microcolony development, downward movements of cellulose at the microcolony surface shape a mushroom-like structure (Video 1, Video S6, Fig. S7). Once this growth period is achieved, the cellulosic lattice brings a great stability to the biofilm and we could not perturb its architecture by increasing the flow rate (Fig. S8).

Fluorescent probes track dynamic changes in cellulose production upon shifts in c-di-GMP signaling

IsoF possesses a type II *bcs* operon similar to the one found in *Escherichia coli*, which is typically under the control of the second messenger cyclic diguanosine monophosphate (c-di-GMP)[28]. Among the nine proteins defining the cellulose synthase complex[29,30], two units, BcsA (*PisoF_03921*) and BcsE (*PisoF_03916*), contain c-di-GMP sensor domains[31,32]. In addition, *PisoF_03915*, the gene directly upstream the *bcs* operon, is a diguanylate cyclase (DGC) that potentially synthesizes c-di-GMP (Fig. 1E). When we overexpressed the *PisoF_03915* gene in IsoF wildtype, the resulting Wt^{PisoF_03915} strain produced biofilms that were clearly distinct from the wildtype (Fig. 4A, B). Wt^{PisoF_03915} biofilms consisted almost exclusively of large, densely packed cell aggregates, which were highly enriched in cellulose but without noticeable fibers or obvious connections to each other and the absence of LS cells – a phenotype compatible with an increased c-di-GMP

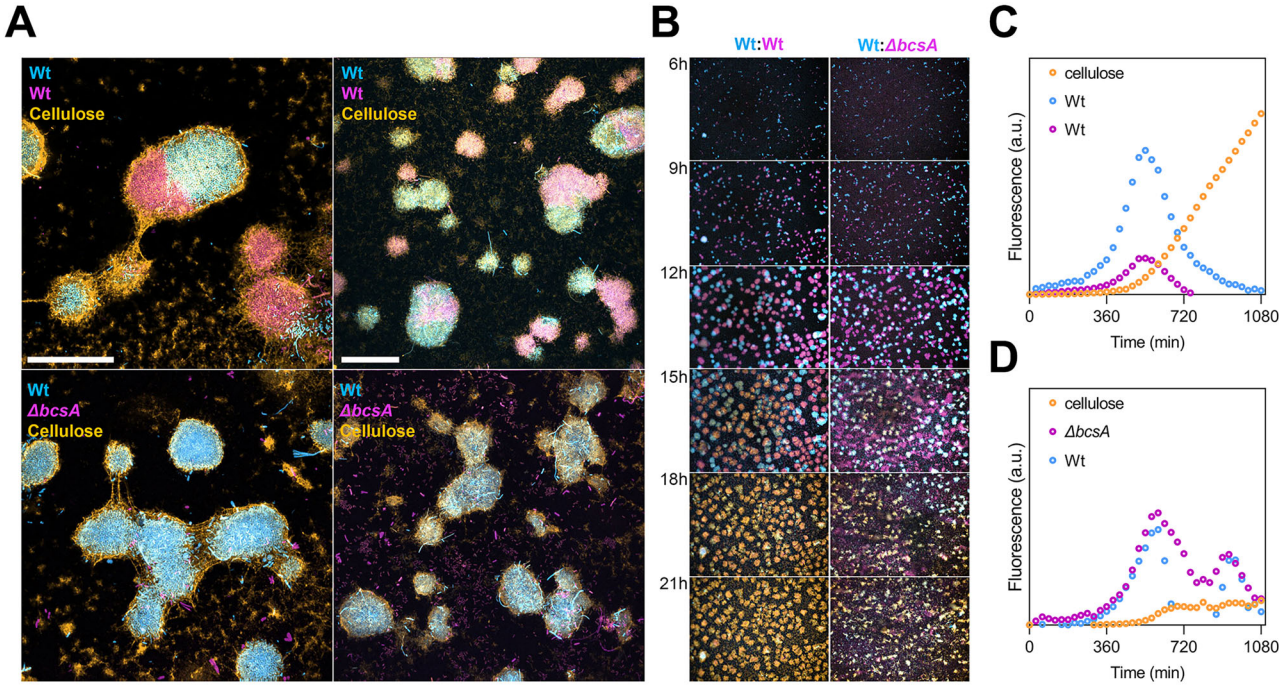

Fig. 5 | Fluorescent labeling reveals cellulose as a private good in IsoF flow-cell biofilms. A Top, mixed biofilms of IsoF wildtype strains marked either with GFP (blue) or mCherry (magenta); cellulose fluorescence (yellow). Cellulose was stained with Compound (**1**). Note that homogenous mixed aggregates rarely occur. Bottom, mixed biofilms of the IsoF wildtype (GFP, blue) and cellulose mutant (Δ*bcsA* mCherry, magenta). Note that Δ*bcsA* cells do not develop stable aggregates. CLSM acquisitions. Bars = 50 µm. **B** Temporal development of mixed biofilms shown in panel A. The lack of cellulose production by Δ*bcsA* cells appears to destabilize the entire biofilm matrix, impacting the wild-type population. Epifluorescence acquisitions. Bar = 50 µm. **C** Quantification of individual fluorophores in mixed Wt:Wt biofilms over time. **D** Quantification of individual fluorophores in mixed Wt: Δ*bcsA* biofilms over time. The washed-away biofilm shows a significantly reduced cellulose production compared to the biofilm formed by the wild-type strains only.

production through the DGC activity of *PisoF_03915* (Fig. 4B). Interestingly, deletion of this gene did not affect biofilm formation in our experimental conditions (Fig. 4B), suggesting that it is not essential to cellulose synthesis in IsoF and that multiple, functionally redundant DGCs may control the activity of the *bcs* operon, as previously reported[33]. We thus artificially increased the global cytosolic levels of c-di-GMP by overexpressing the exogenous *yedQ* gene (DGC) of *E. coli* TG1[34] in the IsoF wildtype strain. In the flow-cell, the resulting Wt^{yedQ} strain produced biofilms similar to those of Wt^{PisoF_03915}, with an apparent enhanced phenotype (Fig. 4A, Fig. S9). In contrast, and as expected, overexpression of the *proE* (PA5295) gene of PAO1 in IsoF, which encodes a phosphodiesterase (PDE) that degrades c-di-GMP[35], led to an impaired biofilm (Fig. 4C). We measured cellulose production of the various IsoF strains as the fluorescence produced by staining with compound (**1**) (Fig. 4D). While in the wildtype a linear increase of the signal was observed after a 6-h lag period, cellulose production increased exponentially in strains harboring high c-di-GMP levels, albeit after a much longer lag phase (14–18 h). In line with c-di-GMP regulation of cellulose production, fluorescence of Wt^{PDE} remained substantially reduced throughout the experiment (Fig. 4D). Collectively, our results show that our fluorophores can reliably monitor changes in cellulose production during biofilm formation, as the measured levels match the expected cellulose amount under native, high and low c-di-GMP levels (Fig. 4D). Further, the stains allow the visualization of the structural development of IsoF biofilms in our flow-cell conditions, canonically relying on the c-di-GMP-controlled cellulose production. CLSM inspections of Wt^{yedQ} aggregates displayed a dense matrix encasing individual cells, a structure that greatly differed from the fibrillar aspect observed in wildtype biofilms, evoking a sponge and reminiscent of EPS materials visualized in *E. coli* AR3110 macrocolonies[36] (Fig. 4E, F). Despite the compact matrix, compound (**1**) consistently penetrated microcolonies and labeled cellulose throughout their interior, indicating that the polysaccharide is uniformly distributed around cells within the aggregates (Fig. S9).

In the absence of cellulose, the Δ*bcsA* FC aggregates develop similar to wildtype aggregates, however, after 4–6 h of growth the mutant aggregates lose cohesion and the cells are washed away by the flow shear forces in the form of filamentous structures (Video S7). Interestingly, although we expected the loss of cellulose production to counteract the effect of a high intracellular c-di-GMP level, the $\Delta alg8,bcsA^{yedQ}$ strain developed a biofilm that was similar to the one formed by Wt^{yedQ} but with slacked aggregates (Fig. 4A, Fig. S10). By contrast, the $\Delta bcsA,pea^{yedQ}$ and $\Delta alg8,bcsA,pea^{yedQ}$ strains were found to be severely impaired in biofilm formation in a manner similar to Δ*bcsA*, suggesting that in IsoF, Pea can compensate for the lack of cellulose production under high c-di-GMP (Fig. S10B). Of note, our data provide evidence that alginate does not contribute to the architecture of IsoF flow-cell grown biofilms in our experimental conditions (Fig. 3).

Fluorescent probes establish cellulose privatization in *Pseudomonas sp.* IsoF biofilms

When two microcolonies grew towards each other they did not merge but stayed separated, indicating that some form of self-recognition is preventing them to mix. As the extracellular matrix can prevent the mixture between colonies[37], we speculated that the cellulose-based matrix of IsoF could act as a physical barrier between the microcolonies. To determine if our fluorescent tools could clarify whether the cellulose-based matrix of IsoF acts as a private good, we inoculated the flow-cells with a mixture of two wildtype derivatives that were labeled with either GFP or mCherry. By growing the mixed biofilm in the presence of compound (**1**), thus allowing multiplexing with GFP and mCherry spectral properties, we observed that microcolonies were predominantly encapsulated in their own matrix (Fig. 5A). When the Δ*bcsA* strain was mixed with the wildtype, the mutant did not integrate into the aggregate network formed by the wildtype, but generated LS-like populations that colonized the void spaces between these aggregates without connecting to the cellulose matrix. As a consequence, the mutant population lacked stability and was eventually washed away by the flow, destabilizing

the entire biofilm (Fig. 5B, D). These results show that compound (**1**) can be deployed with commonly used fluorescent markers and indicate that cellulose is not a common good in IsoF, in line with a previous report in *P. aeruginosa* PAO1, showing that the exopolysaccharide Psl cannot be exploited by a Psl null mutant[38]. According to our results, cellulose defines a border which confines self from non-self-populations in our flow-cell grown biofilms and its production not only ensures adherence to the entire substratum, but also warrants the structural integrity of the entire biofilm population. As the absence of ECM contribution by Δ*bcsA* populations brings the whole mixed biofilm to collapse, we propose that the wildtype biofilm growth sequence consisting of irreversible attachment and matrix production by FC cells is repeated by LS cells after their seemingly stochastic leave out of FC aggregates. LS growth and cellulose contribution are then limited by space constraints but are intrinsic to biofilm stability.

Cellulose or Pea overproduction triggers artefactual biofilm behaviors in *Pseudomonas sp*. IsoF visualized by fluorescent probing

In flow-cells, Wt^{yedQ} produces a compact matrix that prevents individual cells from exiting the aggregates (Fig. 4E, F, Fig. S10A–B). We reasoned that elevated cytosolic c-di-GMP pools enforce cellulose production at the single cell level that translates into cell-to-cell adherence. In line with this, cellulose overproduction sites were evident on single planktonic Wt^{yedQ} cells immobilized on nutrient agar (Fig. S11A), and subsequent growth led to aggregative behaviors where dividing cells firmly encased into a dense cellulose lattice (Fig. S11B). This behavior was also observed in overnight liquid cultures of strains with high c-di-GMP levels, where cells sedimented (Fig. S11C). While the Δ*bcsA,pea*^{yedQ} and Δ*alg8,bcsA,pea*^{yedQ} cultures remained turbid despite the high c-di-GMP conditions, Wt^{yedQ}, Δ*alg8*^{yedQ}, Δ*bcsA*^{yedQ}, Δ*pea*^{yedQ}, Δ*alg8,pea*^{yedQ}, and Δ*alg8,bcsA*^{yedQ} cultures sedimented. Autoaggregation assays indicated these phenotypes were due to cellulose and/or Pea overproduction (Fig. S11C), as previously reported for other polysaccharides in several strains[39–45]. As expected, staining of Wt^{yedQ} sedimented clumps with compound (**1**) and subsequent microscopic inspection showed large aggregates where cells were firmly enclosed into cellulose (Fig. S11D).

Bacterial colonies on agar plates are well-established biofilm models, with exopolysaccharides affecting colony morphology being hallmarks of c-di-GMP signaling[46–48]. We thus assessed alginate, cellulose, and Pea contribution to colony morphology under native and high c-di-GMP conditions on agar plates supplemented with compound (**2**), which stains cellulose with a visible, intense red coloration. After 80 hours of growth, IsoF wildtype and its derived exopolysaccharide mutants showed a smooth unstained phenotype (Fig. 6A), which indicates that these polysaccharides are not produced in significant amounts on agar plates under native c-di-GMP conditions (Fig. 6B). Under high c-di-GMP, macrocolony development led to wrinkled morphotypes, with stiff Wt^{yedQ} colonies showing densely packed cells in a cellulose lattice (Fig. 6B, C), similar to structures observed in *E. coli* K-12 AR3110[36,49]. All strains overproducing only cellulose, or cellulose and Pea (Wt^{yedQ}, Δ*alg8*^{yedQ}, Δ*pea*^{yedQ}, Δ*alg8,pea*^{yedQ}) showed a cellulose-positive rugose phenotype (Fig. 6A), while the strains overproducing only Pea (Δ*bcsA*^{yedQ}, Δ*alg8,bcsA*^{yedQ}) showed an unstained spreading phenotype with radial wrinkles (Fig. 6A). It is interesting to note that KT2440 macrocolonies expressing yedQ remained unstained and did not display the IsoF Wt^{yedQ} morphotype, but resembled the morphologies of IsoF Δ*bcsA* mutants microcolonies under high c-di-GMP conditions (Fig. S12). These results establish the utility of compound (**2**) for observing and measuring cellulose production in macrocolony assays, and confirm that Pea and cellulose overproduction shape IsoF macrocolonies under high c-di-GMP.

Similarly, we leveraged the propensity of IsoF to form pellicles under native and high c-di-GMP conditions. Although compound (**1**) gave satisfactory imaging quality of the cellulose matrix in flow-cell chamber biofilms, it was not the case for pellicles or macrocolonies, as its fluorescent properties were too close to the ones of pyoverdine[50], whose encoding genetic region occurs in IsoF's genome (*PisoF_03299-PisoF_03304*) (Fig. S13A–C). However, we could exploit compound (**2**), which displays fluorescent properties compatible with visualization and quantification of cellulose-specific fluorescence in these settings (Fig. 6D, Fig. S13A, D–F). Microscopy of native pellicles showed interconnected cellulose fibrils and self-embedded microcolonies, resembling flow-cell biofilms architectures (Fig. 6E, Fig. 2A, Fig. S2, Video S8). Under native c-di-GMP levels, only the Δ*bcsA* mutation showed altered pellicles compared to wildtype, confirming the importance of cellulose for pellicle formation in IsoF under our experimental conditions (Fig. 6D). As in agar colonies and flow-cell biofilms, high c-di-GMP triggered a shift towards a denser matrix architecture (Fig. 6F), and the role of Pea only became noticeable under high c-di-GMP levels and the absence of cellulose[51]. While Pea provides the pellicle a remarkable structural resilience compared to cellulose (Video S9), cellulose increases the propensity of the pellicles to sediment (Video S10).

Taken together, our results demonstrate the suitability of compound (**2**) for assessing cellulose production in macrocolonies and pellicles, and underline the important structural role of cellulose in these IsoF biofilms as well as the remarkable conservation of its 3D structural development across discrete biofilm models. However, in native conditions, we did not find substantial amounts of labeled cellulose fibers in shaking or solid culture media, suggesting that these environments do not trigger c-di-GMP-dependent architectures. Conversely, artificially raising the cytosolic levels of this second messenger imposes a sessile regime to IsoF cells that translates into a unique, dense matrix architecture in all biofilm models tested, with cellulose as the primary material.

Discussion

While a number of studies have investigated the spatial distribution of biofilm matrix materials, information on their temporal production is scarce. In most studies, simply snapshots at single time points have been investigated. Only recently, novel approaches and setups have been employed to combine spatial and temporal expression patterns to shed light on the dynamics of biofilm structural development[52–58]. Limiting factors in these studies are often the restricted penetration of matrix-targeting stains within dense biofilms (*e.g.* lectin-based fluorophores), limited specificity and selectivity and potential toxicity. Here we identified and used stable, non-phototoxic fluorescent molecules that accurately labeled cellulose without disrupting the biofilm structural integrity. We showed that these stains are suitable for continuous, dynamic imaging of biofilm development with deep diffusion into inner layers.

By employing these tools, we achieved a cost-effective, high quality temporal and spatial resolution visualization of the formation of cellulose-based biofilms using IsoF as a model. Through manipulation of intracellular c-di-GMP levels, these stains proved to be suitable for tracking real-time changes in cellulose matrix production during biofilm formation. Our work also shows that cellulose defines the 3D architecture of IsoF's matrix across diverse biofilm models. Although the production of the secondary exopolysaccharide Pea is responsive to artificial increases in c-di-GMP, its physiological function and regulation remain unclear. Given the varying environmental conditions and physicochemical parameters across the different biofilm models, it is likely that distinct external stimuli converge to modulate intracellular c-di-GMP levels, acting as a critical checkpoint in the control of biofilm growth. Moreover, the striking similarities between IsoF's flow-cell and pellicle matrix architectures suggest that a unique biological sequence is triggered once this checkpoint is reached, likely involving the same molecular components for biofilm initiation and construction. While low external stress maintains matrix production at basal levels, convergent microenvironmental conditions within microcolonies (*e.g.* oxidative stress, nutrient limitation, shear forces) might drive the alignment of c-di-GMP-dependent cellular responses. An alternative explanation is that IsoF may, akin to *psl* regulation in *P. aeruginosa*[43], involve a cellulose-triggered feedback loop enhancing c-di-GMP signaling. Although we have not yet substantiated this hypothesis, it represents a promising direction for future investigation. However, our data also highlight that artificially raising c-di-GMP contents, a common practice to increase the production of matrix

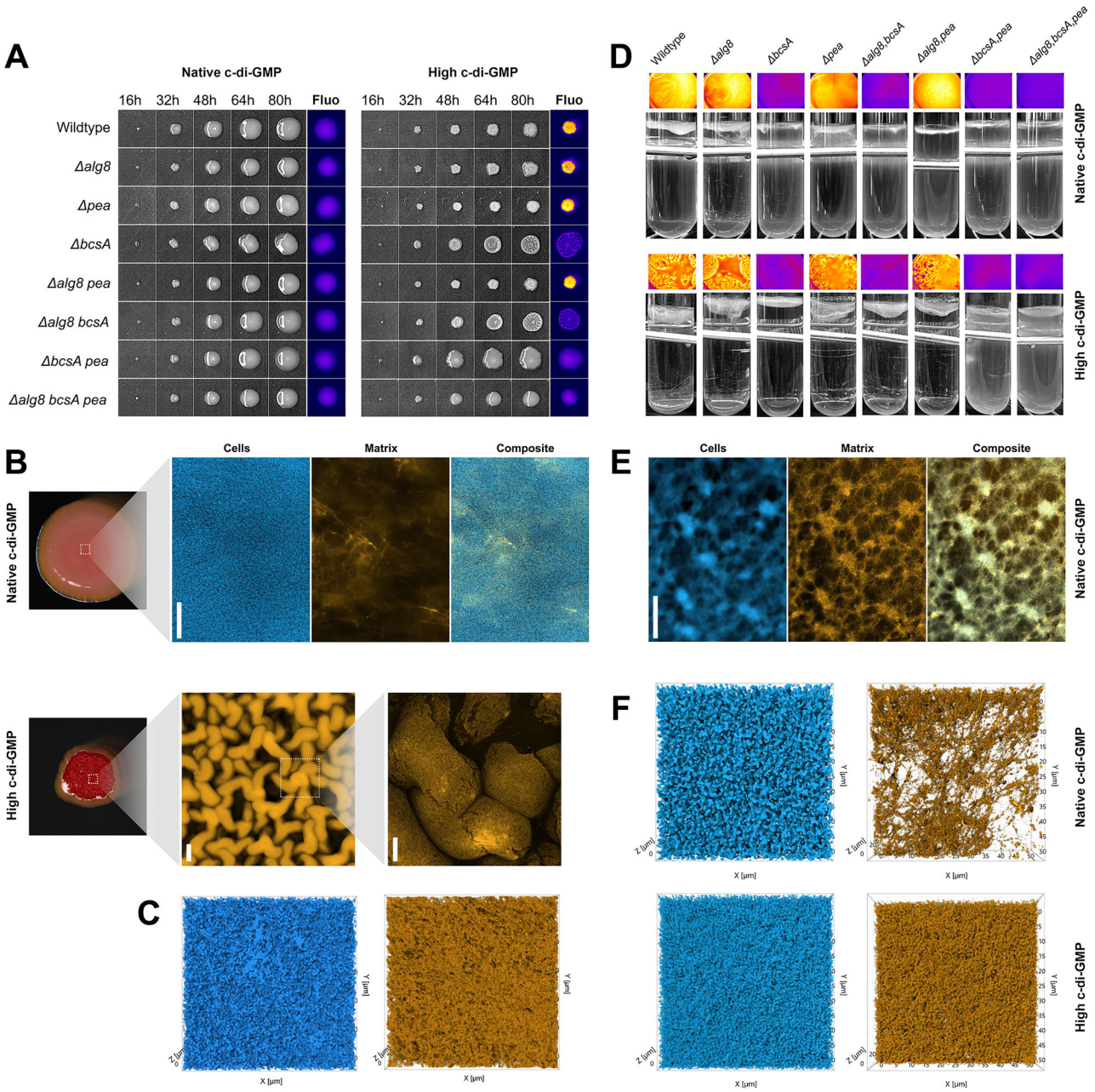

Fig. 6 | Increased c-di-GMP levels similarly alter the matrix-dependent morphogeny of IsoF macrocolonies and pellicles, as visualized by fluorescent labeling. A Representative developmental sequences of toothpick-inoculated colonies of Wt and indicated mutants under native and high c-di-GMP levels. The Fluo panel displays Compound (**2**) fluorescence after 80 h of growth, Fire LUT. Bar = 5 mm (**B**) 3-day old toothpick-inoculated colonies grown on solid medium supplemented with Compound (**2**). Top row displays a Wt colony and representative micrographs of its population; note the presence of low-abundant and disordered cellulose fibers. Bar = 50 µm. Bottom, from left to right: a Wt^{yedQ} colony showing Compound (**2**) uptake and wrinkly morphotype; magnification of the wrinkles (Bar = 200 µm); CLSM maximum projection of the wrinkly surface (Bar = 100 µm). **C** Top view CLSM shadow projections of Wt^{yedQ} wrinkly surface, 50 × 50 µm. Note the dense packing of cells and the compact cellulose matrix. **D** Top and side views of 48h-old pellicles of the Wt and indicated mutants under native and high c-di-GMP levels. Compound (**2**) fluorescence is shown, Fire LUT. Note the clear liquid column under established pellicles, indicating that most cells populate the air-liquid interface. **E** Top view of a wildtype pellicle at meso scale. The structural development of the pellicle matrix remarkably resembles the one observed in flow-cell grown biofilms (see Fig. 2). Bar = 200 µm (**F**) Top view CLSM shadow projections of Wt (top) and Wt^{yedQ} (bottom) pellicles, 50 × 50 µm. Note the fibrillar matrix in native conditions versus the dense, spongy architecture under high c-di-GMP conditions. SYTO9-stained (**B**, **C**, **F**) or GFP-expressing (**E**) cells are shown in blue, the cellulose matrix in yellow.

polysaccharides, results in the formation of biofilms that substantially differ in structure from the ones formed by the wildtype under native c-di-GMP levels, and thus has only limited predictive value for understanding biofilm matrix dynamics and architecture. It is acknowledged that the flexible transitions between planktonic and biofilm stages are modulated by localized c-di-GMP signaling in response to external cues[33]. Therefore, we believe that the fluorescent probes described here will facilitate the identification of input- and output-specific c-di-GMP signaling proteins in bacterial biofilms relying on cellulose. Furthermore, live-monitoring of cellulose architectures will enable the direct investigation of the detachment mechanisms involved in biofilm dispersal and the fate of matrix polysaccharides at this stage of the biofilm cycle. Finally, the interplay between

polysaccharides and other matrix components, such as proteins and extracellular DNA, in shaping biofilm architecture and functionality requires further work. We foresee our fluorescent probes could grant access to this knowledge, for their spectral properties are compatible with a wide range of fluorescent proteins and specialized fluorophores. The potential of these compounds for super-resolution microscopy applications will require the attention of specialists, however, some prerequisite including high photostability, brightness and functionality in aqueous environments and live-cell conditions, are already at hand.

Our screen for small fluorescent molecules that stain different matrix materials identified several compounds that show great promise to visualize the production of some polymeric substances within biofilms in real time, with distinct spectral properties and high multiplexing potential. We are currently exploring the specificity of some of these compounds and testing their applicability to study the biofilm development in diverse bacteria to identify the general principles that govern the spatiotemporal production of extracellular polymers shaping biofilm structures, and how these affect the physiology of biofilm cells.

Methods

Bacterial growth conditions, plasmids and media

The bacterial strains, plasmids and primers used in this study are listed in Tables S1, S2 and S3, respectively. *Escherichia coli* was used as a host for the plasmid constructs and was routinely grown on Lysogeny Broth (LB, Difco, 240210) at 37 °C and 220 rpm. IsoF overnight cultures were grown in LB at 30 °C and 220 rpm. Flow-cell chamber experiments were performed in AB medium[59] supplemented with 0.1 mM sodium citrate (ABC medium). If indicated, ABC was supplemented with Fluorescent Brightener 134 (compound (**1**); Synthesia) or Tubantin Scarlet 4 G (compound (**2**), CHT group) (working concentrations indicated in Fig. S4). For growth curves in 96-microwell plates, overnight cell cultures were adjusted to an OD600 nm of 0.01 a.u., and 200 µL were inoculated per well. Measurements were taken every 15 min. For mutant selection or transconjugants, *Pseudomonas* isolation agar (PIA, Difco, 292710) was used. If applicable, antibiotics were added at the following final concentrations: 20 µg mL^{-1} tetracycline (Tet), 20 µg mL^{-1} gentamycin (Gm) and 50 µg mL^{-1} kanamycin (Km).

Bioinformatics

Nucleotide and protein sequence searches were done using the Pseudomonas Genome Database (https://www.pseudomonas.com/) and the National Center for Biotechnology Information (NCBI) database (https://www.ncbi.nlm.nih.gov/).

Strain manipulation

Deletion mutants were constructed using SceI-based mutagenesis in which the pGPI-SceI plasmid contains a tetracycline cassette[15]. First, DNA fragments of approximately 500–700 pb, corresponding to the 5′ and 3′ flanking regions of the region targeted to be deleted, were amplified and cloned into the pGPI-SceI::Tet plasmid by restriction enzyme sites. Then, the plasmid was introduced in IsoF via triparental conjugation and integrated into the genome by single homologous recombination. After this, the IsoF single-crossover strain was used for conjugation with *E. coli* pDAI-SceI::Gm, which contains a plasmid that carries the I-SceI nuclease. The I-SceI nuclease produces a double-strand DNA break at its recognition site in the pGPI plasmid, linearizing the chromosome and promoting a second homologous recombination event that can result either in the wildtype or the mutant genotype. For all conjugations, the pRK2013 helper plasmid was used to provide the genes encoding the conjugation machinery. The colonies that lose the pGPI plasmid after the second conjugation step are screened by PCR using check primers, and the PCR result is sequenced. Then, the pDAI-SceI::Gm plasmid was cured. All primers and restrictions enzymes used for cloning are listed in Table S3. The pBBR1MCS5::*yedQ* plasmid was introduced into IsoF wildtype and derived polysaccharide mutants also via triparental conjugation using *Escherichia coli* DH5α as a donor and the *Escherichia coli* DH5α pRK2013 as a helper strain.

Screening of dye collection

The screening of an in-house dye collection to identify suitable candidate fluorophores for visualizing IsoF ECM exopolysaccharide architecture at a high resolution involved pellicle formation assays (see protocol below) conducted in the presence of individual fluorescent compounds (20 µg mL^{-1}). Samples of the pellicles were visualized with a Leica DM6000B epifluorescence microscope at various excitation/emission settings to obtain satisfactory imaging. Compound (**1**), Fluorescent Brightener 134 (CAS 3426-43-5), was defined as a standard for cellulose staining for its bright fluorescence and photostability at low UV (405 nm) excitation energies. Compound (**2**), Tubantin Scarlet 4 G (CHT group), was employed for colorimetric assays, macrocolony assays, pellicle staining and when high spatiotemporal confocal resolution was required to minimize laser phototoxicity (532 nm excitation).

Determining the excitation and emission spectral properties of compounds (1) and (2)

Pellicles of strains Δ*alg8,pea*^{yedQ} (cellulose overproducer), Δ*alg8,bcsA*^{yedQ} (Pea overproducer) and Δ*alg8,pea,bcsA*^{yedQ} (lacking biofilm exopolysaccharides) were grown in a 48-well microplate for 2 days in LB supplemented with 2 µg mL^{-1} of compound (**1**) or 50 µg mL^{-1} of compound (**2**), in presence of 50 µm $FeCl_3$ to reduce pyoverdine-dependent background UV fluorescence. Incubation was done in the dark, at room temperature and under static conditions. Following incubation, fluorescence emission intensities (320–700 nm range, 10 nm increments) were measured at discrete excitation wavelengths (300–600 nm, 10 nm increments) using a top-reading plate reader (BioTek Synergy H1). Three independent experiments, each with three technical replicates, were performed.

Flow-cell chamber experiments

To study biofilm formation live, custom flow-cell chamber devices (4.5 cm length, 3 mm width, 1 mm depth) were first disinfected for 4 h using a 2.5% hypochlorite solution. Thereafter, the system was washed with sterile distilled water overnight. Briefly, the chambers were inoculated with bacterial cell cultures at a low cell density (OD_{600nm} = 0.01, which corresponds to 10^6 $CFU.ml^{-1}$), unless otherwise specified. In competition experiments, cultures of competing strains were adjusted to an OD600 of 0.01 and mixed 1:1. After inoculation, flow-cells were incubated without flow for 90 min to allow cell attachment. After attachment, the flow was started. Biofilms were grown at room temperature (25 °C) under continuous flow of ABC liquid medium at a rate of 0.13 $ml.min^{-1}$ using a Watson-Marlow 205U/CA peristaltic pump equipped with marprene tubes (2.29 mm bore size).

Fluorescence microscopy analyses

For 2D time-lapse acquisitions in which polysaccharide production was tracked over time, compound (**1**) was added into the medium at a final concentration of 1 $µg.ml^{-1}$ and biofilm formation was followed every 10 min for up to 48 hours with a Leica DM6000B epifluorescence microscope. For super high temporal time-lapse experiments, cell division was followed every 5 s for up to 15 h using only the bright field channel. A minimum of two independent experiments were performed per strain. For 3D time-lapse acquisitions in which polysaccharide production was tracked over time, compound (**2**) was added into the medium at a final concentration of 1 $µg.ml^{-1}$ and biofilm formation was followed every 30 min for 24 h with a Leica TCS SPE confocal microscope. Compared to compound (**1**), compound (**2**) minimizes laser phototoxicity. Acquisitions were analysed either with the Leica Application Suite, the Imaris v9.6.0 software package (Bitplane) or Fiji (https://fiji.sc/). SYTO9 and FM4-64 staining procedures were performed according to manufacturer indications (Thermo Fisher Scientific). Delaunay triangulations were performed in Fiji on whole field of view micrographs, defining the microcolonies as point-selected maxima (prominence >20, excluding edge maxima); neighbor analysis was performed using the BioVoxxel toolbox. Measurements of fluorescence were performed on the whole field of view at fixed acquisition settings.

Cellulase treatment

To establish the polysaccharidic nature of the stained matrix in *Pseudomonas sp*. IsoF, 3-day-old flow-cell biofilms previously stained with compound (**1**) were subjected to an overnight treatment with cellulase from *Trichoderma reesei* ATCC 26921 (Sigma-Aldrich). For this purpose, the flow was halted in two distinct channels (treatment and control), and 300 µl of either cellulase (stock: 5 mg mL^{-1} and 8 U mg^{-1}) or water was introduced into the respective channels. Following the overnight treatment, the flow was resumed, and biofilms were visualized under the epifluorescence microscope. Three independent experiments were performed per strain.

Colony morphology on agar plates

To assess the colony morphology and polysaccharide synthesis on agar plates, precultures were grown overnight in LB medium at 30 °C and 220 rpm. Then, cell cultures were adjusted to $OD_{600\ nm}$ 0.1 with LB, and the tips of sterile toothpicks previously dipped into the adjusted culture and dried for 30 s were used to touch-inoculate the plates. LB medium (without salts) with 1.5% agar (w/v) and supplemented with 50 µg mL^{-1} of compound (**2**). Compound (**2**) was used for these experiments because its specific visible and fluorescent properties were compatible with direct observations and the ET-DSRed filter cube in the equipment. Incubation was done at room temperature in the dark for up to 80 h. A minimum of two independent experiments, each with at least two technical replicates, were performed. Images were taken using the Leica DFC7000T fluorescence microscope.

Pellicle formation assays

To study pellicle formation, precultures were grown overnight in LB medium at 30 °C and 220 rpm. To allow pellicle formation, either test tubes or 48-microwell plates containing 5 and 1 mL of LB (without salts) per well, respectively, were inoculated at a final concentration of $OD_{600nm} = 0.01$ (which corresponds to 10^6 CFU.ml^{-1}). The tubes/microwell plates were incubated in standing conditions in the dark and at room temperature (25 °C) for 48 h. Three independent experiments were performed. In order to perform principal component analysis, we obtained fluorescence and bright field acquisitions of pellicles grown in 48-well plates using a Leica DFC7000T fluorescence microscope equipped with an ET-DSRed filter cube. Image features of both channels (mean gray levels, standard deviation, modal gray, minimum gray, maximum gray, median gray, skewness and Kurtosis) were computed from the whole field of view using FiJi.

Bacterial cell auto-aggregation measurement

To assess the contribution of each polysaccharide to cell-to-cell interactions, we determined the absorbance at 600 nm of the upper portion of cell cultures from both IsoF wildtype and its derived polysaccharide mutants. These cultures were grown overnight at 30 °C and 220 rpm, under conditions of both native and high c-di-GMP levels. A higher level of cell precipitation corresponds to a reduced absorbance in the upper portion of the cell cultures, as the precipitating cells settle at the bottom of the tubes.

Statistical analysis

All statistical tests were performed in GraphPad Prism 9.

Data availability

The data that support the findings of this study are available from the corresponding authors. All data needed to evaluate the conclusions in the manuscript are present in the manuscript and/or the Supplementary Materials. The bacterial strains listed in this manuscript can be provided by LE's lab upon reasonable request. Requests should be directed to AB or LE.

Received: 28 May 2025; Accepted: 9 December 2025;
Published online: 09 January 2026

References

1. Flemming, H. C. et al. The biofilm matrix: multitasking in a shared space. *Nat. Rev. Microbiol.* **21**, 70–86. https://doi.org/10.1038/s41579-022-00791-0 (2023).
2. Flemming, H. C. & Wuertz, S. Bacteria and archaea on Earth and their abundance in biofilms. *Nat. Rev. Microbiol.* **17**, 247–260. https://doi.org/10.1038/s41579-019-0158-9 (2019).
3. Morris, C. E. & Monier, J. M. The ecological significance of biofilm formation by plant-associated bacteria. *Annu. Rev. Phytopathol.* **41**, 429–453. https://doi.org/10.1146/annurev.phyto.41.022103.134521 (2003).
4. Balcázar, J. L., Subirats, J. & Borrego, C. M. The role of biofilms as environmental reservoirs of antibiotic resistance. *Front. Microbiol.* **6**, 1216. https://doi.org/10.3389/fmicb.2015.01216 (2015).
5. Mishra, S. et al. Biofilm-mediated bioremediation is a powerful tool for the removal of environmental pollutants. *Chemosphere* **294**, 133609. https://doi.org/10.1016/j.chemosphere.2022.133609 (2022).
6. Vickery, K. Special issue: microbial biofilms in healthcare: formation, prevention and treatment. *Mater. (Basel)* **12**, 2001. https://doi.org/10.3390/ma12122001 (2019).
7. Carrascosa, C., Raheem, D., Ramos, F., Saraiva, A. & Raposo, A. Microbial biofilms in the food industry—a comprehensive review. *Int. J. Environ. Res. Public Health* **18**, 2014. https://doi.org/10.3390/ijerph18042014 (2021).
8. Lebeaux, D., Ghigo, J. M. & Beloin, C. Biofilm-related infections: bridging the gap between clinical management and fundamental aspects of recalcitrance toward antibiotics. *Microbiol. Mol. Biol. Rev.* **78**, 510–543. https://doi.org/10.1128/MMBR.00013-14 (2014).
9. Trubenová, B., Roizman, D., Moter, A., Rolff, J. & Regoes, R. R. Population genetics, biofilm recalcitrance, and antibiotic resistance evolution. *Trends Microbiol.* **30**, 841–852. https://doi.org/10.1016/j.tim.2022.02.005 (2022).
10. Steinberg, N. & Kolodkin-Gal, I. The matrix reloaded: probing the extracellular matrix synchronizes bacterial communities. *J. Bacteriol.* **197**, 2092–2103. https://doi.org/10.1128/JB.02516-14 (2015).
11. Karygianni, L., Ren, Z., Koo, H. & Thurnheer, T. Biofilm matrixome: extracellular components in structured microbial communities. *Trends Microbiol.* **28**, 668–681. https://doi.org/10.1016/j.tim.2020.03.016 (2020).
12. Ghafoor, A., Hay, I. D. & Rehm, B. H. Role of exopolysaccharides in *Pseudomonas aeruginosa* biofilm formation and architecture. *Appl. Environ. Microbiol.* **77**, 5238–5246. https://doi.org/10.1128/AEM.00637-11 (2011).
13. Jennings, L. K. et al. Pel is a cationic exopolysaccharide that cross-links extracellular DNA in the *Pseudomonas aeruginosa* biofilm matrix. *Proc. Natl. Acad. Sci. USA* **112**, 11353–11358. https://doi.org/10.1073/pnas.1503058112 (2015).
14. Steidle, A. et al. Visualization of N-acylhomoserine lactone-mediated cell-cell communication between bacteria colonizing the tomato rhizosphere. *Appl. Environ. Microbiol.* **67**, 5761–5770. https://doi.org/10.1128/AEM.67.12.5761-5770.2001 (2001).
15. Purtschert-Montenegro, G. et al. *Pseudomonas putida* mediates bacterial killing, biofilm invasion and biocontrol with a type IVB secretion system. *Nat. Microbiol.* **7**, 1547–1557. https://doi.org/10.1038/s41564-022-01209-6 (2022).
16. Schuhegger, R. et al. Induction of systemic resistance in tomato by N-acyl-L-homoserine lactone-producing rhizosphere bacteria. *Plant Cell Environ.* **29**, 909–918. https://doi.org/10.1111/j.1365-3040.2005.01471.x (2006).
17. Cárcamo-Oyarce, G., Lumjiaktase, P., Kümmerli, R. & Eberl, L. Quorum sensing triggers the stochastic escape of individual cells from *Pseudomonas putida* biofilms. *Nat. Commun.* **6**, 5945. https://doi.org/10.1038/ncomms6945 (2015).
18. Heredia-Ponce, Z. et al. Genotoxic stress stimulates eDNA release via explosive cell lysis and thereby promotes streamer formation of

Burkholderia cenocepacia H111 cultured in a microfluidic device. *NPJ Biofilms Microbiomes* **9**, 96. https://doi.org/10.1038/s41522-023-00464-7 (2023).
19. Stewart, P. S. Mini-review: convection around biofilms. *Biofouling* **28**, 187–198. https://doi.org/10.1080/08927014.2012.662641 (2012).
20. Ma, L. et al. Assembly and development of the *Pseudomonas aeruginosa* biofilm matrix. *PLoS Pathog.* **5**, e1000354. https://doi.org/10.1371/journal.ppat.1000354 (2009).
21. Webb, J. S. et al. Cell death in *Pseudomonas aeruginosa* biofilm development. *J. Bacteriol.* **185**, 4585–4592. https://doi.org/10.1128/JB.185.15.4585-4592.2003 (2003).
22. Passos da Silva, D. et al. The *Pseudomonas aeruginosa* lectin LecB binds to the exopolysaccharide Psl and stabilizes the biofilm matrix. *Nat. Commun.* **10**, 2183. https://doi.org/10.1038/s41467-019-10201-4 (2019).
23. Dohnalkova, A. C. et al. Imaging hydrated microbial extracellular polymers: comparative analysis by electron microscopy. *Appl. Environ. Microbiol*. **77.** https://doi.org/10.1128/AEM.02001-10 (2011).
24. Nilsson, M. et al. Influence of putative exopolysaccharide genes on *Pseudomonas putida* KT2440 biofilm stability. *Environ. Microbiol.* **13**, 1357–1369. https://doi.org/10.1111/j.1462-2920.2011.02447.x (2011).
25. Fang, X. et al. GIL, a new c-di-GMP-binding protein domain involved in regulation of cellulose synthesis in enterobacteria. *Mol. Microbiol.* **3**, 439–452. https://doi.org/10.1111/mmi.12672 (2014).
26. Heredia-Ponce, Z. et al. Biological role of EPS from *Pseudomonas syringae* pv. syringae UMAF0158 extracellular matrix, focusing on a Psl-like polysaccharide. *NPJ Biofilms Microbiomes* **6**, 37. https://doi.org/10.1038/s41522-020-00148-6 (2020).
27. Heredia-Ponce, Z. et al. Role of extracellular matrix components in the formation of biofilms and their contribution to the biocontrol activity of *Pseudomonas chlororaphis* PCL1606. *Environ. Microbiol.* **23**, 2086–2101. https://doi.org/10.1111/1462-2920.15355 (2021).
28. Römling, U., Galperin, M. Y. & Gomelsky, M. Cyclic di-GMP: the first 25 years of a universal bacterial second messenger. *Microbiol. Mol. Biol. Rev.* **77**, 1–52. https://doi.org/10.1128/MMBR.00043-12 (2013).
29. Krasteva, P. V. et al. Insights into the structure and assembly of a bacterial cellulose secretion system. *Nat. Commun.* **8**, 2065. https://doi.org/10.1038/s41467-017-01523-2 (2017).
30. Acheson, J. F., Ho, R., Goularte, N. F., Cegelski, L. & Zimmer, J. Molecular organization of the *E. coli* cellulose synthase macrocomplex. *Nat. Struct. Mol. Biol.* **28**, 310–318. https://doi.org/10.1038/s41594-021-00569-7 (2021).
31. Zouhir, S., Perchat, S., Nicaise, M., Perez, J. & Guimaraes, B. Peptide-binding dependent conformational changes regulate the transcriptional activity of the quorum-sensor NprR. *Nucleic Acids Res.* **41**, 7920–7933. https://doi.org/10.1093/nar/gkt546 (2013).
32. Morgan, J. L., McNamara, J. T. & Zimmer, J. Mechanism of activation of bacterial cellulose synthase by cyclic di-GMP. *Nat. Struct. Mol. Biol.* **21**, 489–496. https://doi.org/10.1038/nsmb.2803 (2014).
33. Richter, A. M. et al. Local c-di-GMP signalling in the control of synthesis of the *E. coli* biofilm exopolysaccharide pEtN-cellulose. *J. Mol. Biol.* **432**, 4576–4595. https://doi.org/10.1016/j.jmb.2020.06.006 (2020).
34. Steiner, E. et al. The BDSF quorum sensing receptor RpfR regulates Bep exopolysaccharide synthesis in *Burkholderia cenocepacia* via interaction with the transcriptional regulator BerB. *NPJ Biofilms Microbiomes* **8**, 93. https://doi.org/10.1038/s41522-022-00356-2 (2022).
35. Feng, Q. et al. Regulation of exopolysaccharide production by ProE, a cyclic-di-GMP phosphodiesterase in *Pseudomonas aeruginosa* PAO1. *Front. Microbiol.* **11**, 1226. https://doi.org/10.3389/fmicb.2020.01226 (2020).
36. Serra, D. O., Richter, A. M., Hengge, R., Cellulose as an architectural element in spatially structured *Escherichia coli* biofilms. *J. Bacteriol*. **195**, https://doi.org/10.1128/jb.00946-13 (2013).
37. Molina-Santiago, C. et al. The extracellular matrix protects *Bacillus subtilis* colonies from *Pseudomonas* invasion and modulates plant co-colonization. *Nat. Commun.* **10**, 1919. https://doi.org/10.1038/s41467-019-09944-x (2019).
38. Irie, Y. et al. The *Pseudomonas aeruginosa* PSL polysaccharide is a social but noncheatable trait in biofilms. *mBio* **8**, e00374-17. https://doi.org/10.1128/mBio.00374-17 (2017).
39. Kirisits, M. J., Prost, L., Starkey, M. & Parsek, M. R. Characterization of colony morphology variants isolated from *Pseudomonas aeruginosa* biofilms. *Appl. Environ. Microbiol.* **71**, 4809–4821. https://doi.org/10.1128/AEM.71.8.4809-4821.2005 (2005).
40. Starkey, M. et al. *Pseudomonas aeruginosa* rugose small-colony variants have adaptations that likely promote persistence in the cystic fibrosis lung. *J. Bacteriol.* **191**, 3492–3503. https://doi.org/10.1128/JB.00119-09 (2009).
41. Colvin, K. M. et al. The Pel and Psl polysaccharides provide *Pseudomonas aeruginosa* structural redundancy within the biofilm matrix. *Environ. Microbiol.* **14**, 1913–1928. https://doi.org/10.1111/j.1462-2920.2011.02657.x (2012).
42. Byrd, M. S. et al. Genetic and biochemical analyses of the *Pseudomonas aeruginosa* Psl exopolysaccharide reveal overlapping roles for polysaccharide synthesis enzymes in Psl and LPS production. *Mol. Microbiol.* **73**, 622–638. https://doi.org/10.1111/j.1365-2958.2009.06795.x (2009).
43. Irie, Y. et al. Self-produced exopolysaccharide is a signal that stimulates biofilm formation in *Pseudomonas aeruginosa*. *Proc. Natl. Acad. Sci. USA* **109**, 20632–20636. https://doi.org/10.1073/pnas.1217993109 (2012).
44. Pérez-Mendoza, D. et al. Novel mixed-linkage β-glucan activated by c-di-GMP in *Sinorhizobium meliloti*. *Proc. Natl. Acad. Sci. USA* **112**, E757–E765. https://doi.org/10.1073/pnas.1421748112 (2015).
45. Kharadi, R. R. & Sundin, G. W. Cyclic-di-GMP regulates autoaggregation through the putative peptidoglycan hydrolase, EagA, and regulates transcription of the znuABC zinc uptake gene cluster in *Erwinia amylovora*. *Front. Microbiol.* **11**, 605265. https://doi.org/10.3389/fmicb.2020.605265 (2020).
46. Spiers, A. J. et al. Cellulose expression in *Pseudomonas fluorescens* SBW25 and other environmental pseudomonads. In *Intech*, Chapter 1. https://doi.org/10.5772/53736 (2013).
47. Fong, J. C. & Yildiz, F. H. The rbmBCDEF gene cluster modulates development of rugose colony morphology and biofilm formation in *Vibrio cholerae*. *J. Bacteriol.* **189**, 2319–2330. https://doi.org/10.1128/JB.01569-06 (2007).
48. Xu, A. et al. Rugose small colony variant and its hyper-biofilm in *Pseudomonas aeruginosa*: adaption, evolution, and biotechnological potential. *Biotechnol. Adv.* **53**, 107862. https://doi.org/10.1016/j.biotechadv.2021.107862 (2021).
49. Serra, D. O., Richter, A. M., Klauck, G., Mika, F. & Hengge, R. Microanatomy at cellular resolution and spatial order of physiological differentiation in a bacterial biofilm. *mBio* **4**, e00103-13. https://doi.org/10.1128/mBio.00103-13 (2013a).
50. Dell'Anno, F., Vitale, G. A., Buonocore, C., Vitale, L. & Palma Esposito, F. Novel insights on pyoverdine: from biosynthesis to biotechnological application. *Int J. Mol. Sci.* **23**, 11507. https://doi.org/10.3390/ijms231911507 (2022).
51. Nie, H. et al. Phenotypic-genotypic analysis of GGDEF/EAL/HD-GYP domain-encoding genes in *Pseudomonas putida*. *Environ. Microbiol Rep.* **12**, 38–48. https://doi.org/10.1111/1758-2229.12808 (2020).
52. Futo, M. & Kostić, T. et al. A novel time-lapse imaging method for studying developing bacterial biofilms. *Sci. Rep.* **12**, 21120. https://doi.org/10.1038/s41598-022-24431-y (2022).

53. Molina-Santiago, C. et al. A noninvasive method for time-lapse imaging of microbial interactions and colony dynamics. *Microbiol Spectr.* **10**, e0093922. https://doi.org/10.1128/spectrum.00939-22 (2022).
54. Lee, L. M., Rosenberg, G. & Rubinstein, S. M. A sequence of developmental events occurs underneath growing *Bacillus subtilis* pellicles. *Front. Microbiol.* **10**, 842. https://doi.org/10.3389/fmicb.2019.00842 (2019).
55. Hartmann, R. et al. Quantitative image analysis of microbial communities with BiofilmQ. *Nat. Microbiol.* **6**, 151–156. https://doi.org/10.1038/s41564-020-00817-4 (2021).
56. Ohmura, T., Skinner, D. J., Neuhaus, K., Choi, G. P. T. & Dunkel, J. In vivo microrheology reveals local elastic and plastic responses inside 3D bacterial biofilms. *Adv. Mater.* **36**, e2314059. https://doi.org/10.1002/adma.202314059 (2024).
57. Yan, J., Fei, C., Mao, S., Moreau, A. & Wingreen, N. S. Mechanical instability and interfacial energy drive biofilm morphogenesis. *eLife* **8**, e43920. https://doi.org/10.7554/eLife.43920 (2019).
58. Krajnc, M. et al. Systems view of *Bacillus subtilis* pellicle development. *npj Biofilms Microbiomes* **8**, 25. https://doi.org/10.1038/s41522-022-00293-0 (2022).
59. Clark, D. J. & Maaløe, O. DNA replication and the division cycle in *Escherichia coli*. *J. Mol. Biol.* **23**, 99–112 (1967).

Acknowledgements

We thank Synthesia (Czeck Republic) for providing us the compound Fluorescent Brightener 134 and CHT Group (Switzerland) for providing us the compound Tubantin Scarlet 4G. We also thank Dr. Ratchara Kalawong for creating the IsoF pyoverdine mutant. The PssUMAF0158 and PCL1606 derived mutant strains were created by Z.H.-P. during her research carried out at the University of Malaga (Spain). This work was supported by the Swiss National Science Foundation (SNSF) project 310030_192800 (LE).

Author contributions

A.B. and L.E. conceptualized and supervised the study; A.B. and Z.H-P. developed the methodology, performed the investigation, wrote the main manuscript text and prepared the figures. L.E. performed funding acquisition. All authors finalized and reviewed the manuscript.

Competing interests

The authors declare no competing interests.

Additional information

Supplementary information The online version contains supplementary material available at https://doi.org/10.1038/s41522-025-00892-7.

Correspondence and requests for materials should be addressed to Aurélien Bailly or Leo Eberl.